

## Bose-Einstein coherence in two-dimensional superfluid $^4\text{He}$

S. O. Diallo,<sup>1,\*</sup> J. V. Pearce,<sup>2,1,†</sup> R. T. Azuah,<sup>3</sup> J. W. Taylor,<sup>4</sup> and H. R. Glyde<sup>1,‡</sup>

<sup>1</sup>*Department of Physics and Astronomy, University of Delaware, Newark, Delaware 19716-2593, USA*

<sup>2</sup>*Institut Laue-Langevin, BP 156, 38042 Grenoble, France*

<sup>3</sup>*NIST Center for Neutron Research, Gaithersburg, Maryland 20899-8562, USA*

<sup>4</sup>*ISIS Spallation Neutron Source, Rutherford Appleton Laboratory, Chilton, Didcot OX11 0QX, United Kingdom*

(Received 7 February 2008; revised manuscript received 2 June 2008; published 15 July 2008)

We present neutron-scattering measurements of the atomic momentum distribution and its Fourier transform, the one-body density matrix (OBDM), in liquid  $^4\text{He}$  films adsorbed in nanoporous MCM-41. The measurements were performed at liquid  $^4\text{He}$  temperatures  $T=0.3$  K and  $T=2.3$  K and saturated vapor pressure (SVP) as a function of filling of the MCM-41. The chief goal is to determine whether the OBDM of nearly two-dimensional (2D) helium films has a tail at low temperatures and to measure the height of the tail. It is also to investigate the 2D-3D crossover and whether the height of the tail is larger in 2D than in 3D as predicted. We are able to determine the tail height at short distances only. In the thinnest films investigated (approximately half of a liquid  $^4\text{He}$  monolayer), we find clear evidence of a tail at  $T=0.3$  K of height  $n_0=(9.34 \pm 3.84)\%$  that is not there at  $T=2.3$  K. The tail height, denoted as  $n_0$ , decreases with filling to  $n_0=(2.45 \pm 2.54)\%$  near full pore filling (nearly 3D). The tail height is larger in 2D than in 3D as predicted although the absolute values are smaller than predicted for bulk 2D and 3D. In 3D,  $n_0$  is the condensate fraction.

DOI: [10.1103/PhysRevB.78.024512](https://doi.org/10.1103/PhysRevB.78.024512)

PACS number(s): 61.05.F-, 67.25.bh, 61.43.Gt

### I. INTRODUCTION

Superfluidity and Bose-Einstein condensation (BEC) in reduced dimensions are topics of continuing fundamental interest.<sup>1–8</sup> The most accessible example of low dimensional Bose systems in nature is  $^4\text{He}$  films adsorbed on porous materials or on flat surfaces.<sup>2,4,8–12</sup> Other topical examples are Cooper pairs of electrons in thin-film superconductors,<sup>13</sup> Josephson junction arrays,<sup>14</sup> sodium atoms in optical and magnetic traps,<sup>5,15</sup> and spin polarized atomic hydrogen.<sup>16</sup>

The order parameter used to characterize coherence properties of Bose systems is the one-body density matrix (OBDM); the Fourier transform of the atomic momentum distribution  $n(\mathbf{k})$ . The OBDM is defined<sup>17</sup> as  $\rho_1(\mathbf{r}, \mathbf{r}') = \langle \Psi^\dagger(\mathbf{r})\Psi(\mathbf{r}') \rangle$ , where  $\Psi(\mathbf{r})$  is the field operator that annihilates a particle at point  $\mathbf{r}$ . In uniform 2D or 3D systems, the OBDM depends only on the distance between  $\mathbf{r}$  and  $\mathbf{r}'$ ;  $\rho_1(\mathbf{r}, 0) = \rho_1(\mathbf{r})$ , where we have taken  $\mathbf{r}' = 0$ . If there is coherence, the probability amplitude does not go to zero at large  $|\mathbf{r}|$ . In 2D when there is coherence, the order parameter has a long algebraically decaying tail at low temperature which becomes infinitely long at  $T=0$  K. In uniform three-dimensional (3D) systems, the tail of the OBDM is flat and the Bose-Einstein condensate fraction  $n_0$  is defined as the height of this flat tail,  $n_0 = \lim_{|\mathbf{r}| \rightarrow \infty} \rho_1(\mathbf{r})$ . In finite sized systems, the OBDM can be expressed in terms of natural single-particle orbitals and the condensate fraction defined as the fraction of atoms in the orbital having highest occupation.<sup>18–20</sup>

In bulk  $^4\text{He}$ , a flat tail with a height  $n_0 \approx 7.25\%$  is observed in the OBDM of the superfluid phase and not in the normal liquid.<sup>21</sup> The relationship between superfluidity and BEC in 3D is well grounded theoretically<sup>20,22</sup> and is supported by modern neutron-scattering data<sup>21</sup> and accurate Monte Carlo calculations<sup>23</sup> which show unambiguously that BEC exists only in the superfluid phase. However, when he-

lium is immersed in porous media and the media is fully filled so that we again have 3D or nearly 3D helium, the transition temperature for superfluidity<sup>24–26</sup>  $T_c$  is suppressed below  $T_\lambda$ . Measurements of the phonon-roton modes show that there is BEC in helium in porous media above  $T_c$ , up to  $T_\lambda$  at saturated vapor pressure ( $p \approx 0$ ) but up to temperatures below  $T_\lambda$  at higher pressure.<sup>12,27–29</sup> The state above  $T_c$  where there is BEC but no superflow is interpreted as a Bose glass phase consisting of islands of BEC in a sea of normal liquid.<sup>12,27–30</sup> In the present measurement, the temperature at which we will look for BEC ( $T=0.3$  K) is well below  $T_c$  and we expect the BEC to be continuous and extended across the sample below  $T_c$ .

Torsional oscillator experiments involving liquid  $^4\text{He}$  films<sup>25,31–33</sup> show clear superfluid responses below a critical temperature  $T_c$ . At equilibrium 2D  $^4\text{He}$  densities, this critical temperature is in the range  $0.55 < T_c < 0.8$  K.<sup>7,31</sup> In 2D, the transition from a normal liquid to a superfluid is associated by Kosterlitz and Thouless<sup>1</sup> with the binding of single vortices into pairs of vortices having opposite circulations. At the transition temperature  $T_c$  where the vortices bind, there is a jump in the superfluid density from zero to a finite value,<sup>9</sup>  $\rho_s(T_c)/\rho = (2m/\hbar^2)kT_c/\pi\rho$ . The binding of vortices into pairs is also associated with the onset of a long-range (large  $|\mathbf{r}|$ ) tail in the order parameter,  $\rho(\mathbf{r})$ . Below  $T_c$ , the OBDM has an algebraically decaying tail  $\rho(\mathbf{r}) \sim 1/|\mathbf{r}|^\eta$ , where  $\eta = mkT/(2\pi\hbar^2\rho_s)$ . At  $T > T_c$ , we anticipate that  $\rho(\mathbf{r})$  can be approximately represented by a Gaussian, perhaps including higher order cumulants as in 3D.<sup>21</sup> At  $T < T_c$ ,  $\rho(\mathbf{r})$  will have similar behavior at small  $|\mathbf{r}|$  plus an algebraic tail. The height of the tail is taken as the value of  $\rho(\mathbf{r})$  at the onset of the tail. The goal of the present measurements is to determine the height of this algebraic tail.

The Bose-Einstein condensate properties of  $^4\text{He}$  near free surfaces<sup>34–37</sup> and in idealized 2D  $^4\text{He}$  systems<sup>4,38</sup> have been extensively studied by computer simulations. Krotschek<sup>34</sup>

simulated a system of  $^4\text{He}$  atoms adsorbed on a planar substrate and reported a condensate value that is significantly larger than that found in bulk superfluid  $^4\text{He}$ . Galli and Reatto<sup>36,39</sup> reported a similar behavior of BEC near surfaces using Monte Carlo techniques. The authors found that while  $n_0$  is enhanced above the bulk  $^4\text{He}$  value, it can be significantly reduced by surface excitations such as ripples.<sup>36,39,40</sup> To clarify this assertion, Draeger and Ceperley<sup>37</sup> simulated a finite-thickness  $^4\text{He}$  slab using path-integral Monte Carlo techniques. They found that as one moves toward the helium surface, the condensate fraction initially increases as the density decreases, as a result of the decreasing effect of He-He interactions. The condensate fraction reaches a maximum value of 93% over short length scales. As the density decreases further, the condensate fraction begins to decrease, possibly due to interaction with ripples at the surface of the slab. In a recent variational Monte Carlo calculation, Marín *et al.*<sup>41</sup> investigated the OBDM in a  $^4\text{He}$  slab system. They reported a value of  $n_0 \approx 100\%$  near the slab surface where the  $^4\text{He}$  density is lower than the bulk  $^4\text{He}$  density. Similar searches<sup>35</sup> for BEC in systems of  $^4\text{He}$  droplets have been performed. These calculations show that at the center of the drop,  $n_0$  is very close to the bulk superfluid  $^4\text{He}$  value,  $n_0 \approx 10\%$ . The condensate starts to increase as one moves away from the center and reaches a maximum value of 22% near the surface of the droplet where the  $^4\text{He}$  density is low. Other relevant calculations<sup>19,42,43</sup> have predicted large values for  $n_0$  of up to 100% at the surface of a liquid of bosons in a trap.

Early investigations of the ground-state properties of 2D liquid and solid  $^4\text{He}$  as a function of density using Monte Carlo and variational methods were reported by Whitlock *et al.*<sup>38</sup> They found that the asymptotic value of the OBDM in a 2D liquid film at zero pressure (density  $\rho = 0.0432$  atoms/ $\text{\AA}^2$ ) is remarkably large, with  $n_0 \approx 44\%$  in one case. Similarly, Ceperley and Pollock<sup>4</sup> have investigated the OBDM of a 2D  $^4\text{He}$  system at several temperatures (below and above the superfluid transition) at the same density using path-integral methods. Their results show that while the OBDM for 2D  $^4\text{He}$  decays algebraically, the decay becomes slow as the temperature is reduced below the superfluid phase, with a large tail height  $n_0 \sim 22\%$ .

In a more recent Monte Carlo calculation based on the Worm algorithm, Boninsegni *et al.*<sup>7</sup> have simulated the OBDM of 2D liquid  $^4\text{He}$ . They found that at  $T \sim 0.6$  K, the OBDM decays so slowly that its tail appears to be nearly flat as in 3D with height  $n_0 \approx 20\%$ . The difference between the calculated 2D OBDM and a genuinely flat OBDM as seen in 3D is hardly distinguishable. The tail at low temperature disappears with increasing temperature.

While there have been numerous calculations of the OBDM of nearly 2D  $^4\text{He}$  systems, very few experiments have been devoted to their study. To date, the only experimental work (to the best of our knowledge) is that of Pearce *et al.*<sup>3</sup> who investigated the OBDM in  $^4\text{He}$  films adsorbed on MgO powder as a function of film thickness. They found a large  $n_0$  which decreases as the number of adsorbed layers is increased; from  $n_0 \approx 13\%$  at low  $^4\text{He}$  coverage to  $n_0 \approx 7\%$  near full filling.

Recent measurements of the single-particle kinetic energy  $\langle K \rangle$  in bulk  $^4\text{He}$  confined in cylindrical nanoporous xerogels

have been reported by Andreani *et al.*<sup>11</sup> They investigated how the pore size of the confining media affects the value of  $\langle K \rangle$  and found that the smaller the pore diameter is, the larger  $\langle K \rangle$  becomes. It is worth pointing out the relevance of this measurement since often the  $\langle K \rangle$  values determined from experiments are used to estimate  $n_0$  in bulk liquid  $^4\text{He}$ .<sup>44</sup> This is briefly discussed in Sec. III A. Another relevant measurement is that of Azuah *et al.*<sup>45</sup> who searched for BEC in bulk  $^4\text{He}$  immersed in porous Vycor. They reported values for both  $n_0$  and  $\langle K \rangle$  comparable to bulk liquid  $^4\text{He}$  values.

In this context, it becomes interesting to measure  $n(\mathbf{k})$  and its Fourier transform, the OBDM, in  $^4\text{He}$  films systems as a function of film thickness. Specific goals are to investigate the height of the tail of the OBDM as the dimensionality of the  $^4\text{He}$  system changes from 2D to 3D and to determine whether the height is greater in 2D or nearly 2D  $^4\text{He}$  than in 3D as predicted.

To measure the momentum distribution of atoms  $n(\mathbf{k})$ , in condensed matter, neutron scattering at high momentum and energy transfers is needed.<sup>46–50</sup> Essentially, for a momentum transfer  $\hbar\mathbf{Q}$  from the neutron to the struck atom, the energy transfer is  $\hbar\omega = \frac{\hbar^2}{2m}((\mathbf{k} + \mathbf{Q})^2 - \mathbf{k}^2) = \frac{\hbar^2}{2m}(\mathbf{Q}^2 + 2\mathbf{k} \cdot \mathbf{Q})$  or  $\omega = (\omega_R + \mathbf{k} \cdot \mathbf{v}_R)$ , where  $\hbar\mathbf{k}$  and  $\hbar(\mathbf{k} + \mathbf{Q})$  are, respectively, the initial and final momenta of the struck atom. This assumes that the struck atom recoils freely where  $\omega_R = \hbar\mathbf{Q}^2/2m$  and  $\mathbf{v}_R = \hbar\mathbf{Q}/m$  are the free-atom recoil frequency and velocity. In this case, the observed dynamic structure factor (DSF) is “Doppler broadened” by the initial momentum distribution of the atoms and is given by<sup>47,49</sup>

$$S_{\text{IA}}(\mathbf{Q}, \omega) = \int d\mathbf{k} n(\mathbf{k}) \delta(\omega - \omega_R - \mathbf{k} \cdot \mathbf{v}_R). \quad (1)$$

In this “impulse approximation”,  $S_{\text{IA}}(\mathbf{Q}, \omega)$  depends only on a single “y scaling” variable  $y = (\omega - \omega_R)/v_R$  and is conveniently expressed as

$$J_{\text{IA}}(y) = v_R S_{\text{IA}}(\mathbf{Q}, \omega) = \int d\mathbf{k} n(\mathbf{k}) \delta(y - k_Q), \quad (2)$$

where  $k_Q = \mathbf{k} \cdot \frac{\mathbf{Q}}{|\mathbf{Q}|}$ .  $J_{\text{IA}}(y)$  is denoted the longitudinal momentum distribution and its Fourier transform,  $J_{\text{IA}}(s)$ , given by

$$J_{\text{IA}}(y) = \int_{-\infty}^{\infty} ds e^{-isy} J_{\text{IA}}(s), \quad (3)$$

is the OBDM for displacements  $s = \mathbf{r} \cdot \hat{\mathbf{Q}}$  along  $\mathbf{Q}$ ,  $\rho_{\text{I}}(s) = J_{\text{IA}}(s)$ .

In real systems, the struck atom does not recoil freely but rather interacts with its neighbors, denoted final-state (FS) effects. Including these FS effects, the exact  $J(Q, y)$  at high  $Q$  is<sup>47</sup>

$$J(Q, y) = \int_{-\infty}^{\infty} ds e^{-isy} J(Q, s), \quad (4)$$

where  $J(Q, s) = J_{\text{IA}}(s)R(Q, s)$  is the exact intermediate scattering function and  $R(Q, s)$  is the final-state function.

Here, we report direct measurements of the height of the tail of the OBDM, denoted as  $n_0$ , in a finite-size 2D  $^4\text{He}$  films at low temperatures. The two dimensionality is ob-

tained by adsorbing  $^4\text{He}$  in the pores of a 45 Å mpd MCM-41. Our central result is that there is a tail in the OBDM at low temperature in films which is not present at high temperature. The coverage dependence of  $n_0$  agrees qualitatively with a previous measurement<sup>3</sup> and several other calculations of  $^4\text{He}$  near a free surface.<sup>37,51</sup>

The article is laid out as follows: The MCM-41 sample and the neutron-scattering experiment are discussed in Sec. II. The fitting procedures and the results are presented in Sec. III, followed by a summary and discussion in Sec. IV.

## II. EXPERIMENTAL DETAILS

The MCM-41 substrate used in the present measurement was synthesized by the group of Michel Soulard at the ‘Laboratoire de Matériaux à porosité contrôlée’ in France, following the procedures described by Corma *et al.*<sup>52</sup> The sample, in the form of a white powder of micrometer size, was characterized by them using  $\text{N}_2$  adsorption-desorption isotherm measurements at 77 K. A standard treatment of these isotherms within the framework of Brunauer, Emmet, and Teller<sup>53</sup> (BET) yields a mean pore diameter (mpd) of 45 Å (with a narrow distribution), a total pore volume of 0.721  $\text{cm}^3/\text{g}$ , and a specific surface area of 645  $\text{m}^2/\text{g}$ . The MCM-41 was chosen as a substrate because of its large surface area and its narrow pore size distribution. Taking advantage of the accurate  $^4\text{He}$  adsorption isotherm measurements by Albergamo *et al.*<sup>54</sup> on a 47 Å mpd MCM-41, it is possible to estimate the  $^4\text{He}$  filling of the present 45 Å mpd sample. The weight of the MCM-41 sample was 32 g.

Before the neutron-scattering measurements, the MCM-41 was outgassed at 120 °C for several hours. The sample was then transferred in a cylindrical Al sample of diameter 43 mm and height 58 mm in a  $^4\text{He}$  atmosphere. The sample cell was aligned with its vertical axis lying in the horizontal relative to the incoming beam in transmission geometry. The cell was attached to an Oxford instruments Heliox VT continuous flow  $^3\text{He}$  sorption cryostat. Temperature reading was provided by a Ge resistance temperature sensors mounted at the top and bottom of the cell and connected to a Neocera temperature controller.

The measurements were carried out at the ISIS spallation neutron source at the Rutherford Appleton Laboratory (U.K.) using the MARI direct geometry time-of-flight (TOF) chopper spectrometer. MARI was set in the high-resolution configuration. A neutron incident energy of  $E_i=750$  meV was selected to allow access to wave vectors up to  $Q < 30$  Å<sup>-1</sup> and energies  $E < 700$  meV. In this setting, the instrumental resolution has been previously determined using accurate Monte Carlo simulations.<sup>21,55</sup> An example of the simulated resolution function at  $Q=26$  Å<sup>-1</sup> is shown in the top panel of Fig. 1 along with the background-subtracted data at the same wave vector.

A preliminary background measurement was performed on the Al sample cell containing the MCM-41 powder only. The actual background used in the data presented here was measured after adsorbing approximately 20 mmol of liquid  $^4\text{He}$  per gram of MCM-41. This filling corresponds approximately to the completion of the first two solidlike or “dead”

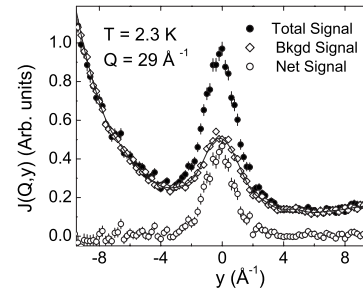


FIG. 1. Net resolution broadened  $J(Q,y)$  (solid circles) at a wave vector transfer of 26 Å<sup>-1</sup> for a filling of 40 mmol/g. Data at temperatures  $T=0.3$  K (Top) and  $T=2.3$  K (Bottom) are shown. The solid lines represents fits to the data as described in the text. The dotted line is the MARI instrumental resolution function at the same wave vector.

layers where superfluidity is not expected to occur.<sup>32,54</sup> Subsequent measurements were performed at SVP and temperatures  $T=0.3$  K and  $T=2.3$  K (above and below the superfluid transition temperature  $T_c$ ) for four layer coverages  $n_{\text{ad}}$ ; respectively, 25, 30, 35, and 40 mmol/g (approximately 42 mmol/g corresponds to full filling). Assuming a concentric and uniform arrangement of the  $^4\text{He}$  atoms inside the MCM-41 pores with the first two layers being solidlike, these fillings correspond to 0.5, 1, 1.5, and 2 liquid layers. The number of  $^4\text{He}$  layers adsorbed on the MCM-41 sample was estimated from this simple picture and from the  $^4\text{He}$  adsorption isotherms measurements of Ref. 54. Since the exact manner in which the layers form is not known, we only quote the actual amount of  $^4\text{He}$  adsorbed onto the sample (coverages) in the remainder of the paper.

Standard procedures<sup>56</sup> were employed to convert the raw scattering data from TOF and intensity to  $\omega$  and the dynamic structure factor  $S(Q, \omega)$ . The data was then converted to the  $y$ -scaling wave vector variable  $y=(\omega-\omega_R)/v_R$  and  $J(Q,y)=v_R S(Q, \omega)$ , as noted above. The results were studied in details in the range  $24 \leq Q \leq 29$  Å<sup>-1</sup> in steps  $\Delta Q=1$  Å<sup>-1</sup>. Figure 2 shows an example of data converted to  $J(Q,y)$  at  $Q=29$  Å<sup>-1</sup> and  $T=2.3$  K at 40 mmol/g filling before and after background subtraction.

## III. ANALYSIS AND RESULTS

### A. Theoretical background

To analyze the data, we express  $J(Q,y)$  as a convolution of the impulse approximation (IA) to  $J(Q,y)$ ,  $J_{\text{IA}}(y)$ , and the FS broadening function  $R(Q,y)$ . This method is denoted as the convolution approach (CA) and is discussed in details in Ref. 47. To determine the condensate fraction, we represent the momentum distribution  $n(\mathbf{k})$  in  $J_{\text{IA}}(y)$  by<sup>21,57</sup>

$$n(\mathbf{k}) = n_0[\delta(\mathbf{k}) + f(\mathbf{k})] + A_1 n^*(\mathbf{k}), \quad (5)$$

where  $n_0\delta(\mathbf{k})$  represents the condensate contribution and  $n^*(\mathbf{k})$  that from states above the condensate ( $k \neq 0$ ). The term  $n_0f(\mathbf{k})$  arises from interactions in liquid helium that lead to scattering of quasiparticles into and out of the condensate to states  $k$  above the condensate. The function  $f(k)$  was derived

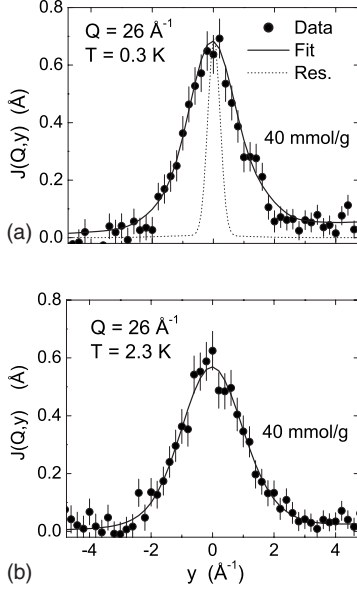


FIG. 2. Observed scattering intensities at 40 mmol/g filling of  ${}^4\text{He}$  (near full filling of MCM-41) at temperature  $T=2.3$  K and wave vector transfer of  $29 \text{ \AA}^{-1}$ . The total neutron-scattering intensity is represented by the solid circles. The background arising from the sample can, the MCM-41 powder, and the first two solid layers (20 mmol/g filling data) are represented by the open diamonds. The solid line shows a smooth fit to this background. The open circles shows the net signal  $J(Q,y)$  from liquid  ${}^4\text{He}$  (background-subtracted data) used in the analysis discussed in the text.

by Gavoret and Nozières<sup>58</sup> and its origin is discussed in Refs. 21 and 57. The  $f(k)$  is highly localized around  $k=0$  and is not accurately known at higher  $k$ . We use the derived  $f(k)$  at low  $k$  with a smooth cutoff at higher  $k$  as fully discussed in Appendix C of Ref. 59 and set out in Eq. (14) of Ref. 21.  $A_1$  is a constant chosen by normalization;  $\int d\mathbf{k}n(\mathbf{k})=1$ . Normalizing  $n(\mathbf{k})$  gives  $n_0[1+I_f]+A_1=1$ , where  $I_f=\int d\mathbf{k}f(\mathbf{k})\approx 0.25$  with the last integral evaluated numerically using the derived  $f(k)$  plus smooth cutoff at higher  $k$ . Including the term  $n_0f(\mathbf{k})$  reduces the value of  $n_0$  obtained from a given set of data by approximately 15%. The OBDM model  $\rho_1(s)$  for displacements  $s=\mathbf{r}\cdot\hat{\mathbf{Q}}$  corresponding to Eq. (5) is

$$\rho_1(s)=n(s)=n_0[1+f(s)]+A_1n^*(s). \quad (6)$$

This OBDM model is depicted in Fig. 3 for  $n_0=9.3\%$ , along with the FS model  $R(Q,s)$  for  $Q=29 \text{ \AA}^{-1}$ . The FS function is essentially unity for  $s<2.5 \text{ \AA}$  and vanishes for  $s>4.5 \text{ \AA}$ . Since the observed scattering function is  $J(Q,s)=n(s)R(Q,s)$ , we can only observe the OBDM up to  $s=4.5 \text{ \AA}$ . Physically,  $R(Q,s)$  depends on the hard core of the atomic pair potential,<sup>60</sup> and much less on the overall density. It is found to be the same in superfluid and normal liquid  ${}^4\text{He}$ , and in solid  ${}^4\text{He}$ . In the present analysis, we use the FS function  $R(Q,s)$  observed in bulk liquid helium at SVP (Ref. 21) even though the density of the helium on MCM at SVP (in different layers) may differ from the bulk density. It is interesting to note that while the calculated OBDM in 3D does show some small amplitude oscillations at short dis-

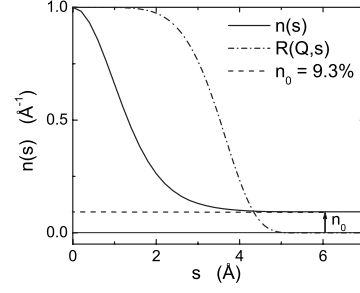


FIG. 3. Model one-body density matrix  $\rho_1(s)=n(s)=n_0[1+f(s)]+A_1n^*(s)$  at filling 25 mmol/g (solid line). Also shown is the condensate component of the model for  $n_0=9.3\%$  (dashed line). The final-state function  $R(Q,s)$  for  $Q=29 \text{ \AA}^{-1}$  is represented by the dash-dotted line. It is zero for  $s>5 \text{ \AA}$ .

tances, the recent OBDM calculations of Boninsegni *et al.*<sup>7</sup> for 2D show essentially no oscillations.

The quality of the current data is only sufficient to determine one parameter reliably. Our initial goal was to determine both the height of the OBDM tail (also known as the condensate parameter  $n_0$ ) and the second moment of  $n^*(\mathbf{k})$ ,  $\bar{\alpha}_2=\int d\mathbf{k}n^*(\mathbf{k})k_Q^2$ , which sets the atomic kinetic energy from the data. Given the statistical quality of the data, we chose to focus only on extracting the condensate parameter  $n_0$ . To do this, we use two methods of analysis.

In a first approach, we use the models (5) and (6). The key assumption of this method is that the second moment of  $n^*(\mathbf{k})$ ,  $\bar{\alpha}_2$ , remains essentially the same in the normal and superfluid phases, as is the case in bulk  ${}^4\text{He}$ .<sup>21</sup> In this method, we first determine  $\bar{\alpha}_2$  from the normal phase data, where  $n_0=0$  and then perform CA fits to the superfluid data to get  $n_0$  by keeping  $\bar{\alpha}_2$  at the value obtained in the normal phase. Again, all other components of  $J(Q,y)$  are kept at their bulk values from Ref. 21 except  $n_0$ .

In an alternative method, we deduce  $n_0$  from the kinetic energy  $\langle K \rangle$ ,  $\langle K \rangle=(3\hbar^2/2m)\bar{\alpha}_2$ , in the normal and superfluid phases, following a method proposed originally by Sears *et al.*<sup>44</sup> (See Refs. 3, 44, and 45 for further details). In the Sears method, it is assumed that all drop in  $\langle K \rangle$  as temperature is lowered into the superfluid phase arises from BEC, giving

$$n_0=\frac{1-\langle K_S \rangle/\langle K_N \rangle}{1+I_f}, \quad (7)$$

where the subscripts  $S$  and  $N$  indicate, respectively, superfluid and normal phases. Since the Sears method is known to overestimate  $n_0$  as well as the associated error,<sup>45</sup> we use it here solely to check qualitatively the CA results.

## B. Results

Figure 2 shows the observed  $J(Q,y)$  of liquid  ${}^4\text{He}$  adsorbed inside the pores of the MCM-41 sample at a filling of 40 mmol/g and temperatures  $T=0.3$  K and  $T=2.3$  K. The statistical precision is comparable to that of our previous measurements of liquid  ${}^4\text{He}$  adsorbed on MgO surface<sup>3</sup> or confined in Vycor.<sup>45</sup> However, in the present experiment, the aim is to determine the height of the OBDM in quasi-2D systems consisting of  ${}^4\text{He}$  films of only few atoms thickness.

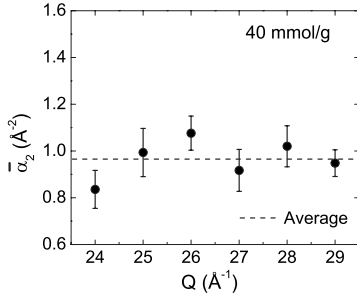


FIG. 4. Typical variation of the parameter  $\bar{\alpha}_2$  with  $Q$  obtained from fits of the CA model to the data at  $T=2.3$  K and near full filling of the MCM-41. The dashed line represents its average value. The fluctuations of  $\bar{\alpha}_2$  with  $Q$  reflect the counting statistical error. The single-particle kinetic energy is  $\langle K \rangle = (3\hbar^2/2m)\bar{\alpha}_2 = 17.45 + 0.55$  K. The bulk liquid  $^4\text{He}$  value is  $\langle K \rangle = 16.30 \pm 0.30$  K (Ref. 21).

This is made possible by the large surface area of the MCM-41 powder which allows more  $^4\text{He}$  atoms (therefore, more scattering centers) to be adsorbed on a single monolayer. We note that the quality of the data is still lower than that of bulk liquid  $^4\text{He}$ .<sup>21</sup>

To obtain the width  $\bar{\alpha}_2$  of  $J(Q, y)$ , which sets the kinetic energy ( $\langle K \rangle \propto \bar{\alpha}_2$ ), we fit the CA method to the data by keeping all other components of  $J_{IA}(y)$  fixed at their values in bulk  $^4\text{He}$ .<sup>21</sup> The FS components are also set at their values in bulk  $^4\text{He}$ .<sup>21</sup> Physically,  $R(Q, y)$  depends on the short-range interaction between pairs of atoms (specifically, it depends on the hard core of the pair potential),<sup>49</sup> and much less on the overall density. It is found to be the same in superfluid and normal liquid  $^4\text{He}$  (differing densities). All indications are that  $R(Q, y)$  will be the same in films, as in the bulk even though it is likely that the density is less than the bulk density near the film surface.

Figure 4 is an illustrative example of the variation of the width  $\bar{\alpha}_2 = \langle k_Q^2 \rangle$  of  $J(Q, y)$  with momentum transfer  $Q$  at 40 mmol/g at  $T=2.3$  K. The data points are obtained from fitting the CA model to the data. Similarly, we studied the variation of  $\bar{\alpha}_2$  with  $Q$  at all fillings and temperatures. The associated kinetic energy  $\langle K \rangle = (3\hbar^2/2m)\bar{\alpha}_2$  are displayed in Table I. The errors quoted reflect the precision in which we are able to determine the mean  $\langle K \rangle$  values for  $24 < Q < 29$   $\text{\AA}^{-1}$ , as shown in Fig. 4. To determine  $\bar{\alpha}_2$  in the superfluid phase, we treat the superfluid data in exactly the same way we treated the normal liquid data. That is, we set  $n_0$  to 0 and kept all CA components of  $J(Q, y)$ , except  $\bar{\alpha}_2$ , fixed at their bulk  $^4\text{He}$  values from Ref. 21 and fitted  $J(Q, y)$  to the data to obtain  $\bar{\alpha}_2$ . The  $\bar{\alpha}_2$  values obtained at  $T=2.3$  and  $T=0.3$  K are shown in Fig. 5.

TABLE I. Single-particle kinetic energy  $\langle K \rangle$  as a function of filling of the MCM-41,  $n_{\text{ad}}$ , at  $T=0.3$  K and  $T=2.3$  K.

$n_{\text{ad}}$ (mmol/g)	25	30	35	40
Liquid layers	0.5	1.0	1.5	2.0
$T=2.3$ K	$17.99 \pm 1.27$	$17.09 \pm 0.73$	$19.63 \pm 0.91$	$17.45 \pm 0.55$
$T=0.3$ K	$15.09 \pm 0.91$	$16.18 \pm 0.91$	$17.82 \pm 1.1$	$16.72 \pm 0.55$

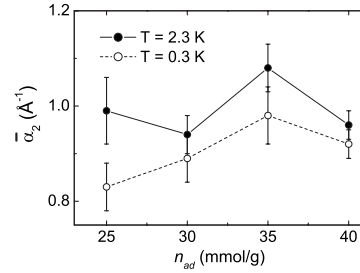


FIG. 5. Average values of the fitted  $\bar{\alpha}_2$  parameter as a function of  $^4\text{He}$  coverage at  $T=2.3$  K (solid circles) and  $T=0.3$  K (open circles). The  $\bar{\alpha}_2$  parameter is consistent with the value found in bulk  $^4\text{He}$  (e.g.,  $\bar{\alpha}_2=0.897$   $\text{\AA}^{-2}$  at  $T=2.3$  K and  $\bar{\alpha}_2=0.884$   $\text{\AA}^{-2}$  at  $T=1.6$  K) (Ref. 21) and appears to be largely independent of  $^4\text{He}$  coverage.

Figure 6 compares the observed OBDM projected along  $s=\mathbf{r} \cdot \hat{\mathbf{Q}}$  at filling of 25 mmol/g at two different temperatures;  $T=0.3$  and  $T=2.3$  K. Our central result is that there is a nearly flat tail in the OBDM at  $T=0.3$  K which is not present at  $T=2.3$  K. In the present analysis and by analogy to the 3D case, the height of this flat tail represents the condensate fraction.

Our results for the OBDM tail height  $n_0$  in liquid  $^4\text{He}$  adsorbed in MCM-41 are summarized in Table II. The variation of  $n_0$  as a function the number of atoms adsorbed in the pores  $n_{\text{ad}}$ , obtained directly from the data assuming the model  $n(\mathbf{k})$  in Eq. (5), is displayed in Fig. 7. The  $n_0$  parameter is clearly larger at low filling and is seen as a larger occupation of the low momentum states in the momentum distribution  $n(\mathbf{k})$  as the temperature is reduced. This is better illustrated in Fig. 8 which compares the fitted  $J(Q, y)$  at  $T=0.3$  K and that at  $T=2.3$  K as a function of filling of the pore. The fits clearly shows that  $J(Q, y)$  is more sharply peaked at low temperature, particularly at low  $^4\text{He}$  fillings. As more  $^4\text{He}$  is adsorbed onto the MCM-41 sample,  $J(Q, y)$  at low temperature is broadened and the difference in the peaks become gradually small. This reduction of  $n_0$  may be due to the disorder introduced by the confining MCM-41.

Figure 9 compares the values of  $n_0$  obtained from the direct method to those deduced from the Sears approach. Both methods offer compelling evidence for an increase in  $n_0$  as filling of the MCM-41 pores, denoted as  $n_{\text{ad}}$ , is reduced. The Sears method gives larger values of  $n_0$ ;  $n_{0\text{Sears}} \approx 13\%$  compared to  $n_{0\text{Direct}} \approx 9\%$  at  $n_{\text{ad}}=25$  mmol/g.

#### IV. DISCUSSION AND SUMMARY

In ideal 2D  $^4\text{He}$  systems at zero pressure, the atomic kinetic energy  $\langle K \rangle$  is expected to be small.<sup>38</sup> Accurate Monte

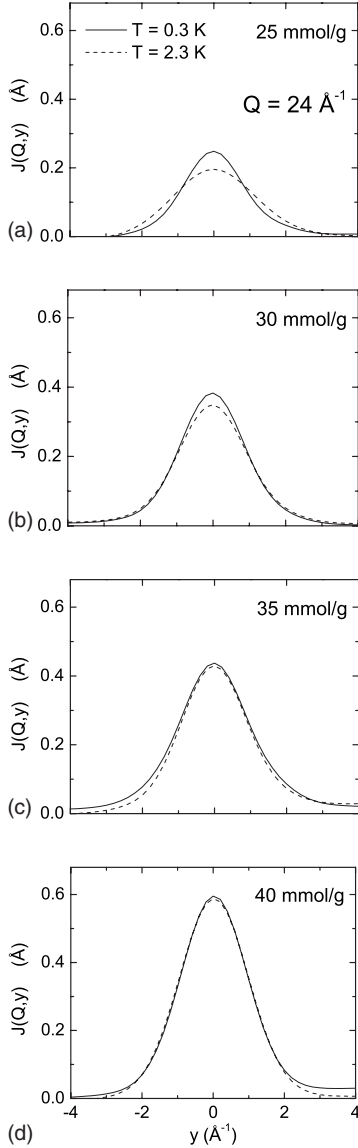


FIG. 6. Observed one-body density matrix  $n(s)$  projected along  $s=\mathbf{r}\cdot\hat{\mathbf{Q}}$  at a filling of 25 mmol/g at temperatures  $T=0.3$  and  $T=2.3$  K. There is a tail in the OBDM at  $T=0.3$  K which is not present at  $T=2.3$  K.

Carlo calculations<sup>4,38</sup> of perfect 2D  $^4\text{He}$  systems show that  $\langle K \rangle$  increases with increasing density; from  $\langle K \rangle=5-6$  K at the 2D equilibrium density  $\rho=0.0432 \text{ \AA}^{-2}$  (zero pressure density) to  $\langle K \rangle \approx 13$  K (Ref. 38) at  $\rho=0.0992 \text{ \AA}^{-2}$ . This is to

TABLE II. Height of the tail of the OBDM,  $n_0$ , as a function of filling of the MCM-41 pores obtained from applying the convolution approach (CA) to the data at  $T=0.3$  K (Direct method) and inferred from the Sears method.

$n_{\text{ad}}$ (mmol/g)	25	30	35	40
Liquid layers	0.5	1.0	1.5	2.0
Direct	$9.34 \pm 3.84$	$3.83 \pm 6.37$	$4.05 \pm 4.12$	$2.45 \pm 2.54$
Sears	$12.93 \pm 8.78$	$4.25 \pm 7.47$	$7.41 \pm 7.80$	$3.33 \pm 4.90$

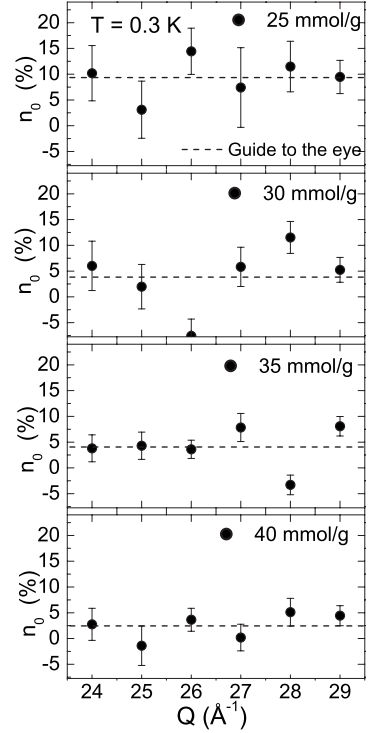


FIG. 7.  $Q$  dependence of the fitted value of the height of the tail of the OBDM ( $n_0$ ) obtained by fitting the convolution approach (CA) at  $T=0.3$  K with the width ( $\bar{\alpha}_2$ ) of  $n(\mathbf{k})$  held fixed at its average value at  $T=2.3$  K shown in Fig. 5.

be compared with the bulk 3D liquid  $^4\text{He}$  value  $\langle K \rangle \approx 16$  K. Within precision, the present observed  $\langle K \rangle$  values of  $^4\text{He}$  confined in the 45  $\text{\AA}$  mpd MCM-41 are comparable to the bulk liquid  $^4\text{He}$  value. This effect has been previously observed in  $^4\text{He}$  adsorbed in 70  $\text{\AA}$  mpd Vycor glass.<sup>45</sup> A possible explanation is that the density of  $^4\text{He}$  confined in the media pores is very similar to that of bulk liquid  $^4\text{He}$ . In fact, recent neutron-scattering measurements (see Ref. 12 and references therein) of the elementary excitation energies of liquid  $^4\text{He}$  in several porous media suggest that the density of  $^4\text{He}$  at partial filling is indeed comparable to bulk liquid density. The temperature dependence of the excitation energies and the widths, which are density dependent, are also the same as in the bulk. It is possible that there are 3D-like

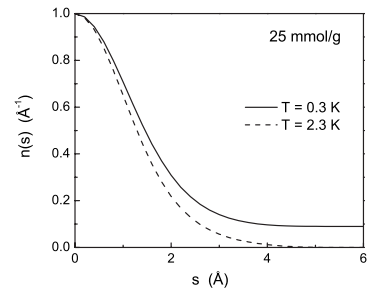


FIG. 8. Representative fits of the CA model of  $J(Q,y)$  to the data at wave vector transfer of  $24 \text{ \AA}^{-1}$ . The fits clearly show that  $J(Q,y)$  at  $T=0.3$  K is more sharply peaked than that at  $T=2.3$  K at low fillings. As more  $^4\text{He}$  is adsorbed onto the MCM-41 sample, the difference in the peak region decreases.

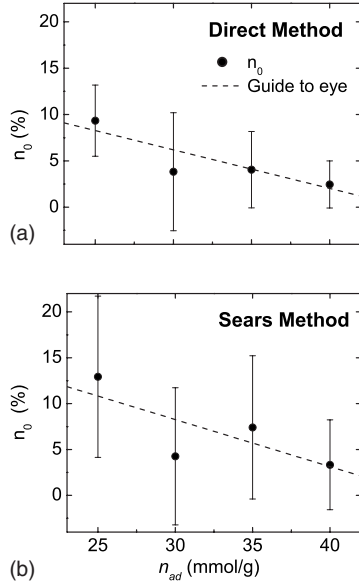


FIG. 9. Height of the tail of the OBDM (BEC parameter)  $n_0$  as a function of  $^4\text{He}$  coverage. The top panel shows the average  $n_0$  values obtained directly from fits of the CA to the data at  $T=0.3$  K (Direct method). The bottom panel shows the values inferred from the drop in the kinetic energy with temperature in the superfluid phase (Sears method). The tail height is clearly larger at low coverage (thin films) than at higher coverage (nearly 3D  $^4\text{He}$ ). The Sears method gives higher  $n_0$  values as expected.

$^4\text{He}$  puddles inside the pores for example. More calculations and measurements of  $\langle K \rangle$  in confined liquid  $^4\text{He}$  systems may clarify this.

We have determined the height of the tail of the OBDM of liquid  $^4\text{He}$  films adsorbed on the pore walls of MCM-41. We find, first, that there is indeed a tail at low temperature ( $T=0.3$  K) in the superfluid phase but not at high temperature ( $T=2.3$  K) in the normal phase ( $T_c \approx 0.65$  K). The height of the tail in films is  $n_0 = 9.83 \pm 3.84\%$ . Our observed value is approximately one half the height ( $n_0 \approx 20\%$ ) predicted by recent PIMC calculations for 2D liquid helium<sup>7</sup> and less than values predicted in earlier calculations.<sup>4,23,34</sup> As the film thickness increases, the height of the tail decreases. At near full filling of the MCM-41 (nearly bulk confined 3D liquid),  $n_0 = 2.45 \pm 2.54\%$ . This value is also close to one half the value of  $n_0$  observed ( $n_0 = 7.25 \pm 0.75\%$ ) (Ref. 21) and calculated ( $n_0 = 7-8\%$ )<sup>7,23,61</sup> for uniform bulk helium. As stated above, the height of the tail  $n_0$  in 3D is the condensate fraction.

Our second conclusion is that the height of the tail of the OBDM is significantly greater in films than in bulk helium as is predicted by calculations for 2D and 3D uniform helium. The absolute values in MCM-41 are less than the predicted but the ratio of the 2D to 3D  $n_0$  values are approximately as predicted. At this time we do not understand why the ob-

served absolute values are less than predicted. In the case of the film, in the calculations,<sup>4,7</sup> an ideal 2D film at its equilibrium density,  $n_A = 0.0432$  atoms per  $\text{\AA}^2$  ( $\text{\AA}^{-2}$ ), was considered. This corresponds to a 3D liquid of density  $n_V = 0.00897 \text{\AA}^{-3}$  which is significantly less than the density of bulk liquid helium at SVP ( $n_V = 0.02186 \text{\AA}^{-3}$ ). The liquid films in MCM-41 are expected to have a density corresponding approximately to the areal density of bulk liquid helium, i.e.,  $n_A = 0.07818 \text{\AA}^{-2}$  which is more than twice the film density used in the calculations. Thus the difference between the calculated and observed  $n_0$  for films may arise simply from a difference in the density of film investigated. In the 3D case, our “fully filled” MCM-41 was not completely filled and therefore not bulk helium. Perhaps not all the liquid helium in the porous media supported a condensate. It could be an effect of confinement to small pore size (45  $\text{\AA}$  in the present case). However, in fully filled Vycor (70  $\text{\AA}$  mpd), we<sup>45</sup> found  $n_0$  comparable to the bulk 3D value.

We have not been able to determine the length of the tail of the OBDM. The observed intermediate dynamic structure factor,  $J(Q, s) = R(Q, s)J_{IA}(s)$ , is the product of the final-state broadening function  $R(Q, s)$  and the OBDM  $J_{IA}(s) = n(s)$ . The FS function goes to zero at  $s \sim 4.5-5 \text{\AA}$ . Thus we can observe the OBDM out to distances  $s \sim 5 \text{\AA}$  only. Out to this distance the tail shape is qualitatively the same in 2D and 3D within the precision of our measurements - with the tail height significantly larger in 2D than 3D. Thus we used the same model of  $n(s)$  to fit the data in 2D and 3D; a constant tail of height  $n_0$ . FS effects can be reduced somewhat by increasing  $Q$ . Extrapolation of our FS function indicates that  $\rho(r)$  could be determined out to  $s = 6-7 \text{\AA}$  at  $Q = 130 \text{\AA}^{-1}$ , for example.

In uniform 3D systems, the tail height is constant out to macroscopic length scales while in 2D the tail decays algebraically with increasing distance  $s$ . However, the tail in real 2D systems is predicted to decay slowly and to extend out to long distances (2–300  $\text{\AA}$ ) at temperatures just below  $T_c$ . In this case, there would be phase coherence over long length scales below but near  $T_c$ , comparable to film sizes in porous media. Our experiments confirm the existence of the tails in 2D. If the tail length is indeed long, then although the origin of superflow in 2D and 3D is different, the onset of superflow in both 2D and 3D is associated with the onset of phase coherence over long length scales. In future experiments, it will be interesting to investigate tail heights at temperatures nearer to  $T_c$ .

## ACKNOWLEDGMENTS

We would like to thank Oleg Kirichek and Richard Down for their assistance on the beamline. Support of this work by the US DOE under Grant No. DE-FG02-03ER46038 and the ISIS neutron facility is gratefully acknowledged.

\*sdiallo@ameslab.gov

†j.v.pearce@npl.co.uk

‡glyde@udel.edu

- <sup>1</sup>J. M. Kosterlitz and D. J. Thouless, *J. Phys. C* **6**, 1181 (1973).
- <sup>2</sup>D. J. Bishop and J. D. Reppy, *Phys. Rev. Lett.* **40**, 1727 (1978).
- <sup>3</sup>J. V. Pearce, S. O. Diallo, H. R. Glyde, R. T. Azuah, T. Arnold, and J. Z. Larese, *J. Phys.: Condens. Matter* **16**, 4391 (2004).
- <sup>4</sup>D. M. Ceperley and E. L. Pollock, *Phys. Rev. B* **39**, 2084 (1989).
- <sup>5</sup>D. Rychtarik, B. Engeser, H.-C. Nägerl, and R. Grimm, *Phys. Rev. Lett.* **92**, 173003 (2004).
- <sup>6</sup>A. Posazhennikova, *Rev. Mod. Phys.* **78**, 1111 (2006).
- <sup>7</sup>M. Boninsegni, N. Prokof'ev, and B. Svistunov, *Phys. Rev. Lett.* **96**, 070601 (2006).
- <sup>8</sup>K. G. Balabanyan, *Phys. Rev. B* **75**, 144512 (2007).
- <sup>9</sup>D. R. Nelson and J. M. Kosterlitz, *Phys. Rev. Lett.* **39**, 1201 (1977).
- <sup>10</sup>I. Rudnick, *Phys. Rev. Lett.* **40**, 1454 (1978).
- <sup>11</sup>C. Andreani, C. Pantalei, and R. Senesi, *Phys. Rev. B* **75**, 064515 (2007).
- <sup>12</sup>F. Albergamo, J. Bossy, J. V. Pearce, H. Schober, and H. R. Glyde, *Phys. Rev. B* **76**, 064503 (2007).
- <sup>13</sup>D. R. Strachan, C. J. Lobb, and R. S. Newrock, *Phys. Rev. B* **67**, 174517 (2003).
- <sup>14</sup>J. Holzer, R. S. Newrock, C. J. Lobb, T. Aouaroun, and S. T. Herbert, *Phys. Rev. B* **63**, 184508 (2001).
- <sup>15</sup>A. Görlitz, J. M. Vogels, A. E. Leanhardt, C. Raman, T. L. Gustavson, J. R. Abo-Shaeer, A. P. Chikkatur, S. Gupta, S. Inouye, T. Rosenband, and W. Ketterle, *Phys. Rev. Lett.* **87**, 130402 (2001).
- <sup>16</sup>A. I. Safonov, S. S. Demoukh, I. I. Safonova, and I. I. Lukashovich, *J. Low Temp. Phys.* **148**, 219 (2007).
- <sup>17</sup>G. Baym, *Lectures on Quantum Mechanics* (Benjamin, London, 1976).
- <sup>18</sup>P. Löwdin, *Phys. Rev.* **97**, 1474 (1955).
- <sup>19</sup>J. L. DuBois and H. R. Glyde, *Phys. Rev. A* **68**, 033602 (2003).
- <sup>20</sup>A. J. Leggett, *Quantum Liquids* (Oxford University Press, New York, 2006).
- <sup>21</sup>H. R. Glyde, R. T. Azuah, and W. G. Stirling, *Phys. Rev. B* **62**, 14337 (2000).
- <sup>22</sup>P. Nozières and D. Pines, *Theory of Quantum Liquids* (Addison-Wesley, Redwood City, CA, 1990), Vol. II.
- <sup>23</sup>D. M. Ceperley, *Rev. Mod. Phys.* **67**, 279 (1995).
- <sup>24</sup>M. H. W. Chan, K. I. Blum, S. Q. Murphy, G. K. S. Wong, and J. D. Reppy, *Phys. Rev. Lett.* **61**, 1950 (1988).
- <sup>25</sup>J. D. Reppy, *J. Low Temp. Phys.* **87**, 205 (1992).
- <sup>26</sup>K. Yamamoto, H. Nakashima, Y. Shibayama, and K. Shirahama, *Phys. Rev. Lett.* **93**, 075302 (2004).
- <sup>27</sup>H. R. Glyde, O. Plantevin, B. Fåk, G. Coddens, P. S. Danielson, and H. Schober, *Phys. Rev. Lett.* **84**, 2646 (2000).
- <sup>28</sup>O. Plantevin, H. R. Glyde, B. Fåk, J. Bossy, F. Albergamo, N. Mulders, and H. Schober, *Phys. Rev. B* **65**, 224505 (2002).
- <sup>29</sup>F. Albergamo, H. R. Glyde, D. R. Daughton, N. Mulders, J. Bossy, and H. Schober, *Phys. Rev. B* **69**, 014514 (2004).
- <sup>30</sup>H. R. Glyde, *Eur. Phys. J. Spec. Top.* **141**, 75 (2007).
- <sup>31</sup>Y. Shibayama and K. Shirahama, *J. Low Temp. Phys.* **148**, 809 (2007).
- <sup>32</sup>Y. Yamato, H. Ikegami, T. Okuno, J. Taniguchi, and N. Wada, *Physica B* **329-333**, 284 (2003).
- <sup>33</sup>H.-C. Chu and G. Williams, *J. Low Temp. Phys.* **138**, 343 (2005).
- <sup>34</sup>E. Krotscheck, *Phys. Rev. B* **32**, 5713 (1985).
- <sup>35</sup>A. Griffin and S. Stringari, *Phys. Rev. Lett.* **76**, 259 (1996).
- <sup>36</sup>D. E. Galli and L. Reatto, *J. Phys.: Condens. Matter* **12**, 6009 (2000).
- <sup>37</sup>E. W. Draeger and D. M. Ceperley, *Phys. Rev. Lett.* **89**, 015301 (2002).
- <sup>38</sup>P. A. Whitlock, G. V. Chester, and M. H. Kalos, *Phys. Rev. B* **38**, 2418 (1988).
- <sup>39</sup>D. E. Galli and L. Reatto, *J. Low Temp. Phys.* **113**, 223 (1998).
- <sup>40</sup>H. J. Lauter, H. Godfrin, V. L. P. Frank, and P. Leiderer, *Phys. Rev. Lett.* **68**, 2484 (1992).
- <sup>41</sup>J. M. Marín, J. Boronat, and J. Casulleras, *Phys. Rev. B* **71**, 144518 (2005).
- <sup>42</sup>C. Gies and D. A. W. Hutchinson, *Phys. Rev. A* **70**, 043606 (2004).
- <sup>43</sup>J. L. DuBois and H. R. Glyde, *Phys. Rev. A* **63**, 023602 (2001).
- <sup>44</sup>V. F. Sears, E. C. Svensson, P. Martel, and A. D. B. Woods, *Phys. Rev. Lett.* **49**, 279 (1982).
- <sup>45</sup>R. T. Azuah, H. R. Glyde, R. Scherm, N. Mulders, and B. Fåk, *J. Low Temp. Phys.* **130**, 557 (2003).
- <sup>46</sup>P. C. Hohenberg and P. M. Platzman, *Phys. Rev.* **152**, 198 (1966).
- <sup>47</sup>H. R. Glyde, *Excitations in Liquid and Solid Helium* (Oxford University Press, Oxford, England, 1994).
- <sup>48</sup>J. Mayers, *J. Low Temp. Phys.* **109**, 135 (1997).
- <sup>49</sup>*Momentum Distributions*, edited by R. N. Silver and P. E. Sokol (Plenum, New York, 1989).
- <sup>50</sup>C. Andreani, D. Colognesi, J. Mayers, G. F. Reiter, and R. Senesi, *Adv. Phys.* **54**, 377 (2005).
- <sup>51</sup>D. S. Lewart, V. R. Pandharipande, and S. C. Pieper, *Phys. Rev. B* **37**, 4950 (1988).
- <sup>52</sup>A. Corma, Q. Kan, M. T. Navarro, J. Pérez-Pariente, and F. Rey, *Chem. Mater.* **9**, 2123 (1997).
- <sup>53</sup>S. Brunauer, P. H. Emmett, and E. Teller, *J. Am. Chem. Soc.* **60**, 309 (1938).
- <sup>54</sup>F. Albergamo, J. Bossy, and H. R. Glyde, *J. Low Temp. Phys.* **138**, 31 (2005).
- <sup>55</sup>C.-K. Loong, S. Ikeda, and J. M. Carpenter, *Nucl. Instrum. Methods Phys. Res. A* **260**, 381 (1987).
- <sup>56</sup>K. H. Andersen, R. Scherm, A. Stunault, B. Fåk, H. Godfrin, and A. J. Dianoux, *J. Phys.: Condens. Matter* **6**, 821 (1994).
- <sup>57</sup>A. Griffin, *Phys. Rev. B* **32**, 3289 (1985).
- <sup>58</sup>J. Gavoret and P. Nozières, *Ann. Phys. (N.Y.)* **28**, 349 (1964).
- <sup>59</sup>H. R. Glyde, *Phys. Rev. B* **50**, 6726 (1994).
- <sup>60</sup>R. N. Silver, *Phys. Rev. B* **38**, 2283 (1988).
- <sup>61</sup>S. Moroni and M. Boninsegni, *J. Low Temp. Phys.* **136**, 129 (2004).